

**Stopping of 5 – 100 keV helium in tantalum, niobium, tungsten, and AISI 316L steel**

P. Haussalo, K. Nordlund and J. Keinonen

*Accelerator Laboratory, P.O. Box 43, FIN-00014 University of Helsinki, Finland*

(October 11, 1995)

The stopping power of Ta, Nb, W, and AISI 316L stainless steel for He ions at velocities below the Bohr velocity has been deduced by comparing the ranges of 5 to 100 keV He<sup>+</sup>-ions determined with the elastic-recoil-detection-analysis method with those obtained in molecular dynamics simulations. The nuclear slowing down was treated through the use of molecular dynamics calculations and a potential obtained from density-functional theory calculations. The comparisons showed that the electronic stopping powers given by J. F. Ziegler, J. P. Biersack, and U. Littmark [*The Stopping Powers and Ranges of Ions in Matter (Pergamon, New York, 1985), Vol. 1*], had to be multiplied with a factor of 1.4 for Ta, 1.0 for Nb, 1.1 for W, and 1.0 for AISI 316L. The uncertainty of the factors and hence the scaled stopping power values is  $\pm 5\%$ . The total stopping powers were obtained from molecular dynamics simulations in which the modified electronic stopping powers were used.

**I. INTRODUCTION**

The tabulation of electronic stopping powers and ranges of all ions in materials is based on the scaling of proton data [1]. Due to the fact that there are very few experimental data in the literature for the low velocity ions (velocity lower than the Bohr velocity  $v_0 \sim c/137$ , where  $c$  is the velocity of light), the tabulated stopping power values are in most cases based on systematics and extrapolation of experimental data. The electronic stopping power for low velocity He ions is of special interest since they are closest to protons and are therefore the first test of the scaling.

All experimental ion range data include both the electronic and nuclear stopping powers of the ions. Our recent studies on molecular dynamics (MD) calculations show that the use of MD simulations and an interatomic potential obtained from the DMol density-functional theory package [2, 3] enables a realistic and accurate treatment of the collisions of slowing down ions with substrate atoms [4]. Thus the nuclear stopping power is treated highly accurately, making it possible to study the electronic stopping power by comparing experimental range results with simulations of range distributions [5].

The aim of this work was to learn more about helium stopping in metals at low velocities. In our studies on mechanisms of hydrogen retention in metals containing helium [6], we have noticed that in many cases standard sources for the stopping data, e.g. the TRIM91 code [1], are not accurate enough in the range of energies (below 100 keV) used in our experiments. New stopping data in this energy range is therefore desirable. To our knowledge there are no experimental electronic stopping data in the literature for He ions in Ta, Nb, W and AISI 316L stainless steel at energies corresponding to velocities below the Bohr velocity.

The stopping power of He ions in tungsten and stainless steel is also of interest because these metals are under consideration for use as structural materials in future fusion

reactors. The energy range below 100 keV is relevant because the fusion plasma temperature corresponds to keV energies [7]. Tantalum and niobium were included in this study since we have previously studied ion implantation induced damage in them, e.g. Refs. [8, 9].

**II. EXPERIMENTAL ARRANGEMENTS**

The samples were prepared by implanting 5-, 20-, 40-, 60-, 80-, and 100-keV <sup>4</sup>He<sup>+</sup> ions into 0.25 mm thick polycrystalline Nb (99.9% pure), Ta (99.9% pure), W (99.95% pure), and AISI 316L stainless steel slices. The AISI 316L steel has a density of 7.96 g/cm<sup>3</sup> and contains iron, 18 % Cr, 10% Ni and 3% Mo and relatively small amounts of carbon [10]. The implantations were performed at room temperature in the 100 keV isotope separator of the laboratory. The implanted fluences were  $1 - 5 \times 10^{16}$  ions cm<sup>-2</sup>. In order to have about the same maximum He concentration in all the samples (about 5 at.% required by the analyzing techniques), the fluence was increased along with the implantation energy. The implantation current varied between 3 and 23  $\mu$ A cm<sup>-2</sup>.

The concentration profile of implanted He was measured by the elastic-recoil-detection-analysis (ERDA) technique [6]. The 25-MeV beam of <sup>16</sup>O<sup>4+</sup> ions used to bombard the samples was generated by the 5 MV tandem accelerator EGP-10-II of the laboratory. The angle between the primary beam direction and the target surface was 20°. Recoils were detected by a 50 mm<sup>2</sup> surface barrier detector (Canberra PIPS) centered at an angle of 40° with respect to the incident beam direction. The detector was masked so that it subtended a solid angle of 60  $\mu$ Sr. A 19  $\mu$ m thick mylar absorber foil was used to separate the recoiled H and He atoms and to discriminate the scattered projectile atoms.

The experimental depth resolution was about 15 nm. It was contributed to by the energy resolution of the detector (15 keV at FWHM), kinematical broadening due

to the solid angle of the detector and straggling of the recoiling atoms in the absorber foil. The accumulated charge was normalized between different measurements by using another 50 mm<sup>2</sup> surface barrier detector located at 170° with respect to the incident beam to count the backscattered beam particles from a tantalum covered, rotating chopper blade. The typical measuring time was about half an hour.

For the recoiled 4.5 – 8.0 MeV He ions coming through the mylar foil to the detector, the energy calibration of the detector was made using a source containing <sup>233</sup>U, <sup>238</sup>Pu, and <sup>239</sup>Pu isotopes. This source emits several 4.7 – 6.8 MeV  $\alpha$ -particles [11], which makes the calibration very accurate. The energy response of the detector was found to be linear.

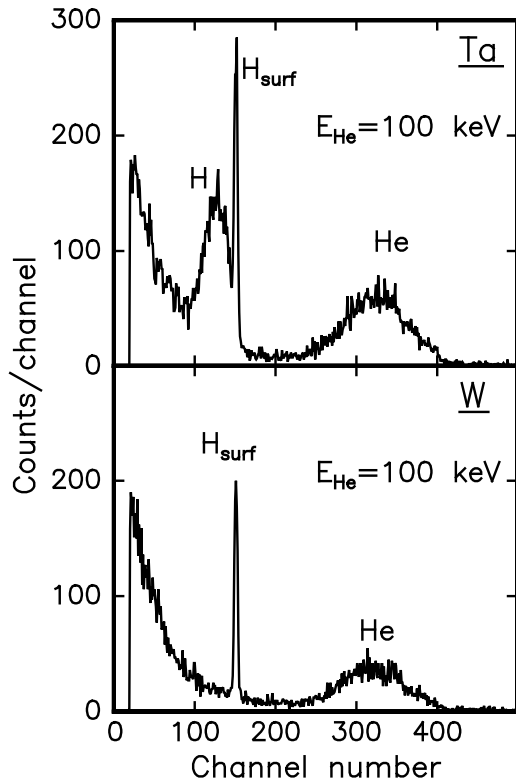


FIG. 1. Typical spectra from ERDA measurements for tantalum and tungsten. The peaks of implanted helium, hydrogen trapped at He, and hydrogen in hydrocarbons at the surface of the sample are marked with He, H, and H<sub>surf</sub>, respectively. The peak to the left of the hydrogen contains other light elements, e.g. carbon. Note that in W there is no hydrogen trapped at the He precipitates.

### III. MEASUREMENTS AND RESULTS

Spectra measured with Ta and W samples are illustrated in Fig. 1. Hydrogen located at the sample surface is indicated in the figure. This peak was used to correct for small gain variations between different measurements.

In Ta and Nb samples hydrogen was observed at the same depth as helium. This can be explained as hydrogen trapped at He precipitates [12]. The hydrogen has migrated there from the metal bulk after the implantation [12]. This is possible because of the very fast diffusion of hydrogen in Ta and Nb at room temperature; the activation energy of migration is only 0.125 – 0.159 eV for Ta [13] and 0.84 eV for Nb [14]. No trapped H was seen at the He precipitates in W and AISI 316L. The activation energy of hydrogen migration in W is 1.4 eV [13]; we did not find any value in the literature for the activation energy for AISI 316L steel.

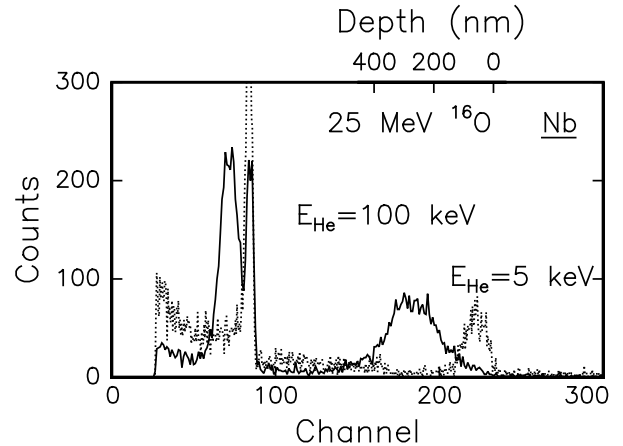


FIG. 2. ERDA spectra of 5- and 100-keV He-implanted niobium samples. The dependence of the He-distribution on the implantation energy is clearly visible.

Fig. 2 shows how the He distribution and its location depend on the energy with which He has been implanted in the sample. The He peak was used to calculate the projected range of He ions in the sample as a function of the implantation energy. The mean He range was obtained as the center of mass of the distribution of implanted He ions. The resulting implantation energy *vs.* mean range data are presented in Figs. 3 and 4 and in Table I.

To deduce the range of the implanted helium from a measured spectrum we had to know the stopping power of a sample for the impinging oxygen beam and recoiling helium atoms, and the stopping power of the mylar foil for recoiling helium atoms. All three stopping powers for the MeV-energy ions are known more accurately than the stopping power for the keV He ions to be deduced [1]. The depth scale of the implanted He was calculated using stopping power tables calculated with TRIM91 [1, 15].

The dependence of the range values on the literature data for MeV-energy stopping powers was studied in the following way. By modifying the MeV-energy stopping powers and recalculating the mean ranges, the change obtained in the mean range was found to be almost the same for all implantation energies. This means that the ef-

fects of possible inaccuracies of the MeV-energy stopping power values on the range values can be minimized by scaling the zero depth of the He distributions. Since the uncertainty of the mean range of the 5-keV distribution is not significant compared to the change in the mean range caused by the inaccuracies of the MeV-energy stopping, the measured and simulated (cf. chapter IV) distributions of 5-keV He implantation were used to scale the zero depth. This procedure resulted in an uncertainty of about 10 nm in the mean ranges.

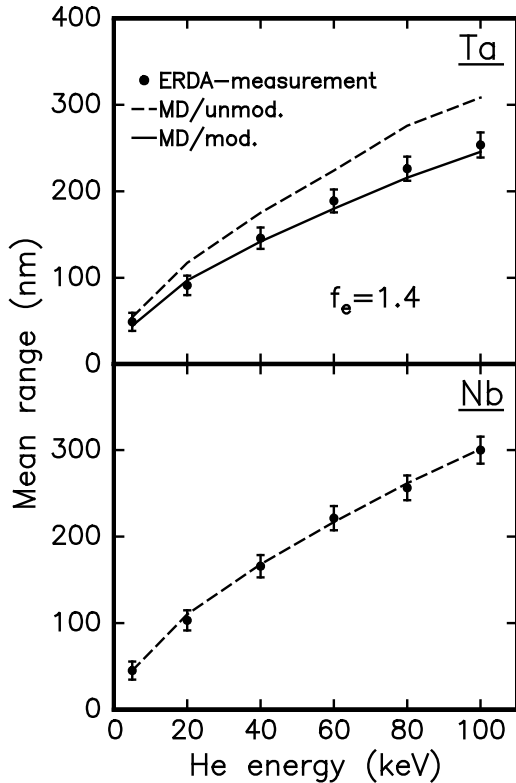


FIG. 3. Mean range of implanted He in tantalum and niobium for the 5 – 100 keV implantations. Mean ranges obtained in MD-simulations with modified and unmodified electronic stopping powers are given by solid and dashed lines, respectively.

The uncertainty of a mean range value obtained in the ERDA measurement also depends on the uncertainty of the measuring angles. When the incident angle decreases, the path of the analyzing beam in the target increases and the path of the recoiling ions reduces. The overall length of the ions increases in the geometry used. Therefore, decreasing the incident angle results in an effect in an ERDA spectrum which is similar to the implanted helium being deeper in the sample. To check how the uncertainty of the depth scale depends on the uncertainty of the angle, we also measured the 100-keV He implanted W and AISI 316L samples using incident angles of 15°, 18°, 22°, and 25° with respect to the sample surface and keeping the detector at 40°. Thus the kinematic factor of He recoils

is kept constant, and differences in detected energy are caused by the different pathlengths the measuring beam and recoiled He ions travel in the target. Calculating mean range values using these measurements we found that the variation in the deduced range values is 2 % for a 1° change of the incident angle, which is the upper limit for the uncertainty of the angle.

The total uncertainty of the experimental range values given in Table I is the sum of the uncertainty of the depth scale and a 2% uncertainty of the incident angle.

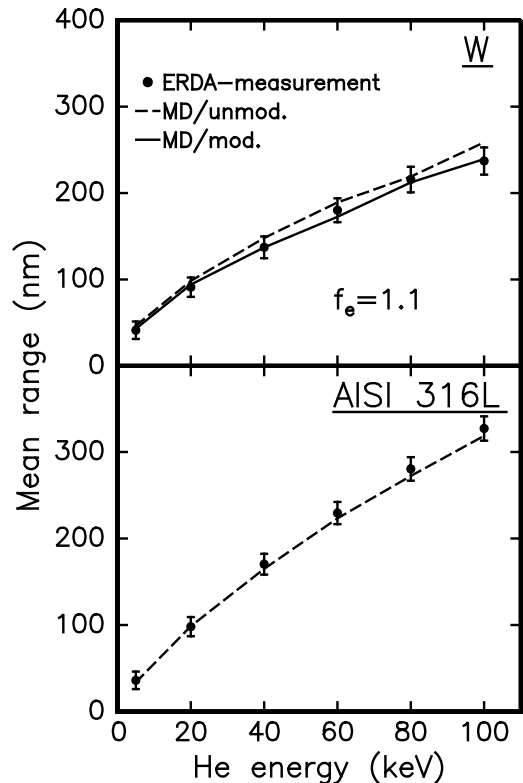


FIG. 4. As for Fig. 3, but for tungsten and AISI 316L stainless steel.

#### IV. SIMULATION OF THE RANGE DISTRIBUTIONS AND THE STOPPING POWER

In the theoretical description of the slowing down of helium ions at keV energies the electronic and nuclear slowing down has to be taken into account. The nuclear slowing down was described by the use of binary collision approximation (BCA) [16] and molecular dynamics (MD) [4] range calculation methods to follow the movement of the implanted ion until it has slowed down to thermal energies. The electronic stopping power was taken into account as a frictional force. The electronic stopping power values were those obtained from TRIM91 [1].

In the range simulations a polycrystalline structure was assumed for the sample, with an average grain size much

larger than the mean range of the He ion. The initial position and direction of the implanted ion when it enters the crystal was selected from a random distribution to take account of all crystal directions in a polycrystalline sample [4]. Before the actual range calculation was started, the atoms were displaced from their ideal lattice sites by an amount which corresponds to thermal movement at room temperature.

TABLE I. Ranges of 5 to 100 keV He atoms

Substrate	Implantation energy (keV)	Mean range (nm)	
		Experimental	Simulated <sup>a</sup>
Ta	5	49±11	44.6±0.4
	20	91±12	97.0±1.2
	40	146±13	142.0±1.2
	60	189±14	179.9±1.2
	80	226±15	216±1
Nb	5	45±11	45.1±0.4
	20	101±12	110±1
	40	166±13	168±2
	60	221±14	216.8±1.2
	80	256±15	262±1
W	5	41±11	43.0±0.5
	20	90±12	94.1±1.2
	40	137±13	137.1±1.2
	60	180±14	173±1
	80	216±14	212±3
AISI 316L	5	36±11	33.8±0.2
	20	98±12	98.7±0.6
	40	170±13	165.0±0.7
	60	229±15	223±1
	80	280±16	272±2
	100	327±17	319±2

<sup>a</sup> MD/DMol calculation. Statistical uncertainty is given.

We first simulated the measured range distribution of the implanted helium using a conventional BCA [16] simulation method. The BCA method was used for the elemental metals tantalum, niobium and tungsten. Ranges in stainless steel were not simulated due to limitations in the BCA simulation code. The repulsive interatomic potential used in the simulations was the one given by Ziegler, Biersack and Littmark (“ZBL”) in Ref. [1].

To obtain a more reliable description of the slowing down, we then proceeded by repeating the range simulations with a new MD method developed at our laboratory [2, 4]. When all physical simulation parameters (the electronic stopping power, the repulsive interatomic potential and the crystal structure) were the same in the MD and

BCA methods, the mean range results differed by no more than  $\pm 6\%$  in this energy range. The difference between BCA and MD simulations utilizing the ZBL potential and TRIM91 electronic stopping power is illustrated in Fig. 5 for Ta, Nb and W. In tantalum and niobium the BCA mean ranges are somewhat shorter than those given by MD, whereas in tungsten the opposite is true. This shows that the different principles used to describe the collision processes in BCA and MD simulations do not result in a systematic difference of the mean ranges for different elements. However, the MD approach is inherently more precise due to the fact that multiple collisions are taken into account realistically and very few unphysical parameters are involved in the simulations [4].

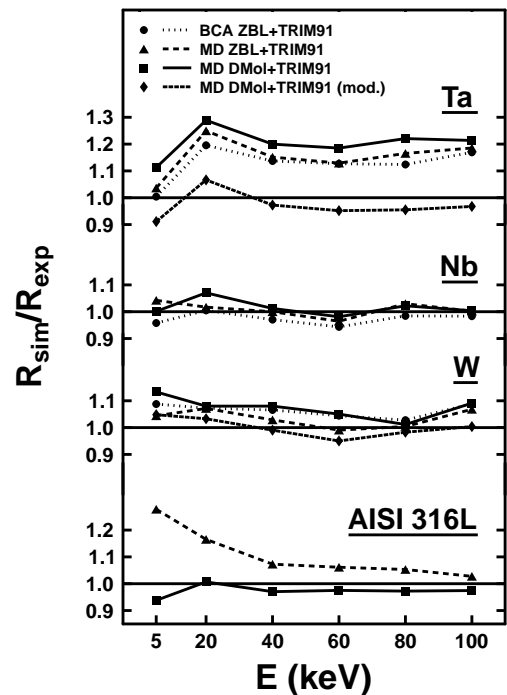


FIG. 5. Comparison of the mean ranges obtained with different simulation methods (BCA and MD) and interatomic potentials (ZBL and DMol) for implantation of He in Ta, Nb, W and AISI 316L stainless steel. The simulated mean ranges have been divided with the experimental mean range results, which correspond to the  $R_{sim}/R_{exp} = 1.0$  lines. Also shown are the ranges obtained with the modified TRIM91 electronic stopping power in Ta and W. In AISI 316L no BCA simulations were carried out.

To further improve the theoretical treatment of the slowing-down process, we used the DMol package [3] to calculate an interatomic repulsive potential for the He – metal interactions. The program utilizes density-functional theory and the local density approximation for electronic exchange and correlation [17]. The calculation principles were similar to those described in Ref. [2]. This procedure yields a more reliable description of the

He – metal interaction than the universal ZBL potential, which is constructed by fitting a universal screening function to potentials calculated for a large variety of atom pairs. From earlier studies [2] and comparison of potentials obtained from density-functional theory and Hartree-Fock *ab initio* calculations we know that the uncertainty of the range data due to interatomic repulsive potentials obtained with the DMol program are much smaller than the uncertainty due to the electronic stopping powers studied in this paper. The mean range results calculated with the DMol potentials were found to differ up to  $\pm 10\%$  from the results obtained with the ZBL potential in Ta, Nb and W (Fig. 5). In stainless steel the difference is very large (up to 35%) at low energies, which may be related to the fact that steel contains the lightest elements used in this study.

The MD/DMol simulations showed that in order to reproduce the experimental range profiles, the electronic stopping power for helium in Ta and W had to be modified. By multiplying the electronic stopping power of Ta and W for He with a constant a good agreement with measurements was obtained at all implantation energies. The multiplying coefficients for the TRIM91 electronic stopping were  $1.4 \pm 0.05$  for Ta and  $1.1 \pm 0.05$  for W. The stopping powers of niobium and AISI 316L stainless steel did not need any modification.

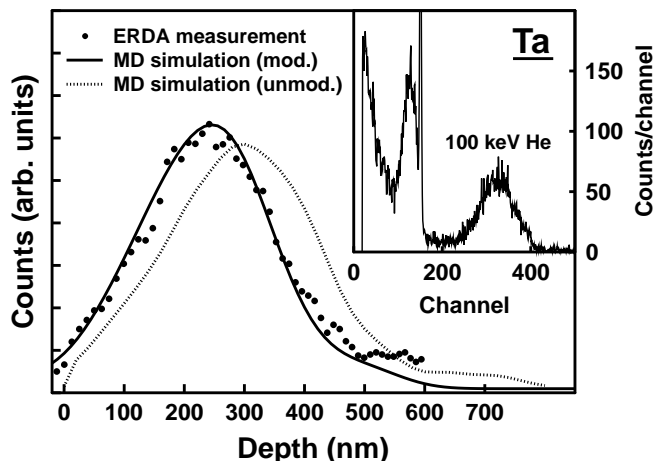


FIG. 6. Measured ERDA spectrum and simulated He distributions for 100 keV implantation in Ta. In the simulation of the modified He distribution, the ZBL electronic stopping has been multiplied with a factor of 1.4. The inset shows the whole ERDA spectrum.

The results of the MD/DMol simulations with modified stopping powers for implantation in Ta and W and unmodified stopping powers for implantation in Nb and steel are compared with the experimental mean range values in Table I. The results are also shown in Figs. 3, 4 and 6. Fig. 6 shows the measured ERDA spectrum and the MD/DMol simulated He distributions for Ta implanted

with 100 keV He-ions.

TABLE II. Total and electronic stopping powers of helium in tantalum, niobium, tungsten and AISI 316L stainless steel obtained in the present work. The nuclear stopping power can be obtained as the difference of the total and electronic stopping powers. The velocity is given in units of the Bohr velocity  $v_0 = 2.19 \times 10^6$  m/s.

$v/v_0$	$S_{\text{tot}}$ (eV/nm)	$S_e$ (eV/nm)	$S_{\text{tot}}$ (eV/nm) $S_e$ (eV/nm)	
			Ta	Nb
0.010	7.33	2.32	8.31	2.30
0.015	8.84	3.49	10.4	3.45
0.020	9.92	4.65	12.1	4.61
0.030	12.6	6.97	15.9	6.91
0.050	18.6	11.6	22.7	11.5
0.080	27.7	18.6	32.7	18.4
0.100	33.6	23.2	38.4	23.0
0.150	46.3	34.9	50.9	34.5
0.200	59.9	46.5	63.8	46.1
0.300	101	87.8	103	87.0
0.500	196	183	194	182
0.800	342	330	337	327
1.000	436	427	425	423
			W	AISI 316L steel
0.010	8.40	2.23	12.9	2.00
0.015	9.46	3.35	16.9	3.00
0.020	10.8	4.46	20.1	4.01
0.030	13.2	6.70	25.3	6.01
0.050	19.0	11.2	34.1	10.0
0.080	28.0	17.9	45.2	16.0
0.100	33.9	22.3	50.9	20.0
0.150	46.5	33.5	62.0	30.0
0.200	60.0	44.6	72.2	40.1
0.300	99.4	84.3	102	75.7
0.500	190	176	176	158
0.800	329	317	297	284
1.000	426	410	381	368

We also calculated the total stopping powers from the MD/DMol simulations. Since the path the ion moves during one time step must be very short in strong collisions in MD simulations [4], we found that it is not practical to calculate the stopping power directly from the definition

$$S_{\text{tot}} = \frac{dE}{dr}. \quad (1)$$

Instead, we calculated the average velocity of the implanted ion as a function of time  $v(t)$  for a large number of recoiling ion histories. From this quantity (which is a smooth steadily decreasing function of  $t$ ) we obtain the stopping power as a function of  $t$

$$S'_{\text{tot}}(t) = -F(t) = -m \frac{dv(t)}{dt}. \quad (2)$$

By inverting the function  $v(t)$  the stopping power as a function of  $v$  can be obtained,

$$S_{\text{tot}}(v) = S'_{\text{tot}}(t(v)) \quad (3)$$

The nuclear stopping power can be obtained as the difference of the total stopping power  $S_{\text{tot}}$  and the modified electronic stopping power  $S_e$ .

In Table II the total and electronic stopping powers deduced in this study are shown for all the studied cases in the energy range 10 eV - 100 keV. The electronic stopping power is the TRIM91 stopping power modified by the scaling factors determined in this study. These modified electronic stopping powers were used in the MD calculations from which the total stopping powers were obtained. Since use of the nuclear stopping power has become largely obsolete due to the availability of BCA and MD simulation methods, we do not give it separately in the table.

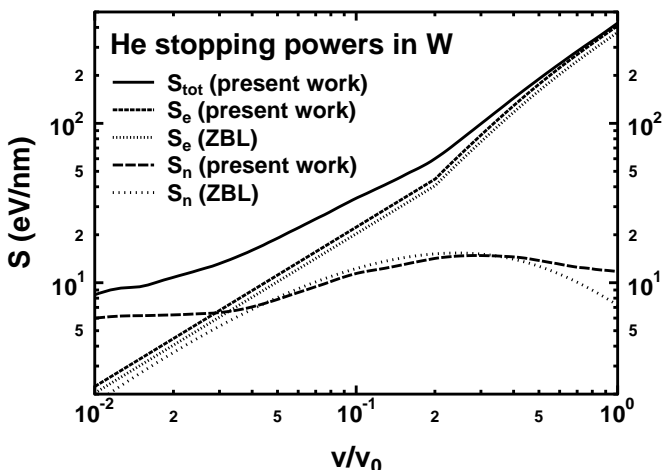


FIG. 7. Total, electronic and nuclear stopping powers of helium in tungsten obtained in the present work. As a reference, also the standard ZBL electronic and nuclear stopping powers are shown in the figure. The velocity range shown corresponds to kinetic energies of 10 eV - 100 keV for the implanted helium ions.

In Fig. 7 the stopping powers obtained in this study are shown along with the standard ZBL stopping powers for the case of helium implantation in tungsten. The difference in the nuclear stopping powers can be attributed to the different interatomic potentials used. At low energies the large difference may also be in part due to the fact that the analytical calculation of the stopping power in the ZBL theory does not take multiple collisions into account.

## V. CONCLUSIONS

The stopping powers of 5 - 100 keV helium in Ta, Nb, W, and stainless steel AISI 316L have been determined experimentally for the first time. The stopping powers were deduced from ion range data by comparing the experimental ranges with the ranges obtained from MD simulations.

The interatomic potentials needed in the calculations to simulate the nuclear stopping powers were obtained from first principle calculations with the DMol package. Range results obtained with the standard ZBL interatomic potential were found to differ up to  $\pm 10\%$  from results obtained with DMol potentials. We also discussed the difference between range results obtained with a conventional BCA simulation method and our novel MD method.

In comparison with the ZBL values the electronic stopping powers have to be multiplied with the factor of  $1.4 \pm 0.05$  for Ta,  $1.0 \pm 0.05$  for Nb,  $1.1 \pm 0.05$  for W, and  $1.0 \pm 0.05$  for AISI 316L stainless steel.

## ACKNOWLEDGEMENTS

This work was supported by the Finnish Ministry of Trade and Industry. One of us (K. Nordlund) wants to thank Dr. A.P. Seitsonen for guidance in using the DMol program.

- 
- [1] J.F. Ziegler, J.P. Biersack, and U. Littmark, *The Stopping and Range of Ions in Solids* (Pergamon, New York, 1985).
  - [2] J. Keinonen, A. Kuronen, K. Nordlund, R.M. Nieminen and A.P. Seitsonen, *Nucl. Instr. Meth. in Phys. Res. B* 88 (1994) 382.
  - [3] DMol is a trademark of Bio Sym. Inc., San Diego, California, USA
  - [4] K. Nordlund, *Comp. Mat. Sci.* 3 (1995) 448.
  - [5] P. Torri, J. Keinonen, and K. Nordlund, *Nucl. Instr. Meth. Phys. Res. B* 84 (1994) 105.
  - [6] P. Haussalo, J. Keinonen, U.-M. Jäske and J. Sievinen, *J. Appl. Phys.* 75 (1994) 7770.
  - [7] ITER plasma facing components (ITER documentation series No. 30, IAEA, Vienna, 1991)
  - [8] J. Keinonen, V. Karttunen, J. Räisänen, F.-J. Bergmeister, A. Luukkainen and P. Tikkanen, *Phys. Rev. B* 34 (1986) 8981.
  - [9] J. Keinonen, A. Kehrel, K.P. Lieb and M. Uhrmacher, *Nucl. Instr. Meth. in Phys. Res. B* 66 (1992) 209.
  - [10] Goodfellow product catalogue 1994/1995, (Goodfellow Ltd, Cambridge, England), p. 303.
  - [11] C.M. Lederer and V.S. Shirley, *Table of isotopes* (Wiley & Sons, New York, 1978).
  - [12] A. Kehrel, J. Keinonen, P. Haussalo, K.P. Lieb and M. Uhrmacher, *Radiat. Eff.* 188 (1991) 297.
  - [13] N.A. Galaktionowa, in *Hydrogen-Metal Systems Data-book*, (Ordentlich, Holan 1981), p. 17, 118.
  - [14] F. Phillipp, B. Saile, K. Urban, in *Point defects and defect interactions in metals*, editors J.I. Takamura, M. Doyama, and M. Kiritani (Univ. Tokyo Press, Tokyo, 1982) p. 261.
  - [15] J.F. Ziegler and J.P. Biersack, TRIM-91 computer code (private communication).
  - [16] M. Hautala, *Phys. Rev. B* 30(1984) 5010.
  - [17] R.O. Jones and O. Gunnarsson, *Rev. Mod. Phys.* 61 (1989) 689.